Published in final edited form as:

Mol Microbiol. 2018 July ; 109(2): 209–224. doi:10.1111/mmi.13978.

THE AER2 RECEPTOR FROM *VIBRIO CHOLERAE* IS A DUAL PAS-HEME OXYGEN SENSOR

Suzanne E. Greer-Phillips[1], **Nattakan Sukomon**[2,3], **Teck Khiang Chua**[3], **Mark S. Johnson**[1], **Brian R. Crane**[3], **Kylie J. Watts**[1,#]

[1]Division of Microbiology and Molecular Genetics, Loma Linda University, Loma Linda, CA, 92350, USA

[3]Department of Chemistry and Chemical Biology, Cornell University, Ithaca, NY, 14850, USA

SUMMARY

The diarrheal pathogen *Vibrio cholerae* navigates complex environments using three chemosensory systems and 44–45 chemoreceptors. Chemosensory cluster II modulates chemotaxis, whereas clusters I and III have unknown functions. Ligands have been identified for only five *V. cholerae* chemoreceptors. Here we report that the cluster III receptor, *Vc*Aer2, binds and responds to O_2. *Vc*Aer2 is an ortholog of *Pseudomonas aeruginosa* Aer2 (*Pa*Aer2), but differs in that *Vc*Aer2 has two, rather than one, N-terminal PAS domain. We have determined that both PAS1 and PAS2 form homodimers and bind penta-coordinate *b*-type heme via an Eη-His residue. Heme binding to PAS1 required the entire PAS core, but receptor function also required the N-terminal cap. PAS2 functioned as an O_2-sensor [$K_{d(O2)}$, 19 μM], utilizing the same Iβ Trp (W276) as *Pa*Aer2 to stabilize O_2. The crystal structure of PAS2-W276L was similar to that of *Pa*Aer2-PAS, but resided in an active conformation mimicking the ligand-bound state, consistent with its signal-on phenotype. PAS1 also bound O_2 [$K_{d(O2)}$, 12 μM], although O_2 binding was stabilized by either a Trp or Tyr residue. Moreover, PAS1 appeared to function as a signal modulator, regulating O_2-mediated signaling from PAS2, and resulting in activation of the cluster III chemosensory pathway.

Graphical abstract

[#]Corresponding author: Telephone: +1 (909) 558-1000 x83394, Fax: +1 (909) 558-4035, kwatts@llu.edu.
[2]Current address: Department of Anesthesiology, Weill Cornell Medical College, New York, NY, 10065, USA

AUTHOR CONTRIBUTIONS

NS and BRC acquired, and TKC refined, the PAS2 structure; SGP and KJW acquired all remaining data; MSJ, BRC and KJW designed this study, interpreted the data, and wrote this manuscript.

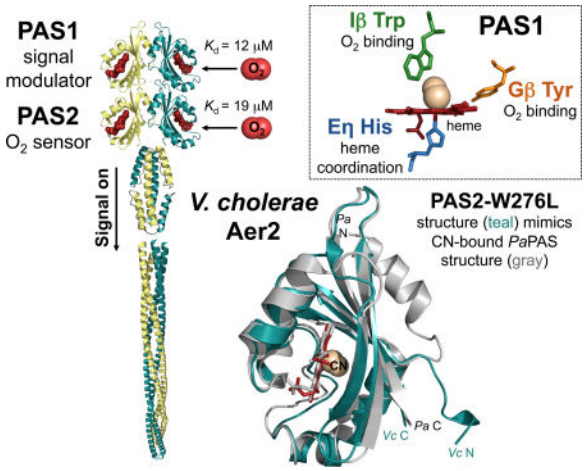

Keywords

Vibrio cholerae ; chemoreceptor; PAS domain; heme; oxygen; signal transduction

INTRODUCTION

*Vibrio cholera*e, the diarrheal pathogen that causes cholera, is a highly motile bacterium that encodes 44 to 45 chemoreceptors and three distinct chemosensory systems (chemosensory clusters I, II and III) (Boin *et al.*, 2004). Chemosensory cluster II expresses a membrane-bound array that modulates bacterial chemotaxis (Gosink *et al.*, 2002, Hyakutake *et al.*, 2005, Briegel *et al.*, 2016). Cluster I functions in microaerobic environments (Hiremath *et al.*, 2015), although its precise role, as well as the role of cluster III, is currently unknown. Cluster III (VCA1089-VCA1096) resides on chromosome II and encodes a complete set of chemosensory proteins (CheY4, CheA3, CheW3, CheW4, CheR3, CheD and CheB3), including a chemoreceptor (VCA1092, Mlp45) that we have named *Vc*Aer2 (Fig. 1A). This designation is based on its homology to the *Pseudomonas aeruginosa* Aer2 receptor (*Pa*Aer2), which we have previously characterized (Airola *et al.*, 2010, Watts *et al.*, 2011, Airola *et al.*, 2013a, Airola *et al.*, 2013b, Garcia *et al.*, 2017). *V. cholerae* cluster III is also orthologous to the *P. aeruginosa* Che2 chemosensory cluster, but includes a second *cheW* gene (Fig. 1A). Notably, the expression of both of these chemosensory clusters i) occurs during stationary phase, ii) requires the alternative sigma factor RpoS, and iii) produces proteins that form polar clusters independent of chemotaxis clusters (Schuster *et al.*, 2004, Guvener *et al.*, 2006, Ringgaard *et al.*, 2015). Cluster III is also expressed in cultures after growth arrest from conditions of carbon starvation or culture saturation (Ringgaard *et al.*, 2015).

The *V. cholerae* chemotaxis system (cluster II) mirrors that of a classic chemotaxis pathway, whereby chemoreceptor signaling activates the autophosphorylation of receptor-bound CheA2, which in turn phosphorylates the response regulator CheY3 (Boin *et al.*, 2004). Phospho-CheY3 then binds to the flagellar motor protein, FliM (Biswas *et al.*, 2013), changing the direction of flagellar rotation from counterclockwise to clockwise, and causing mono-flagellated *V. cholerae* to reverse its direction. In contrast to Cluster II, the Cluster III

components CheA3, CheW3, and CheY4 do not support chemotaxis in *V. cholerae* (Gosink *et al.*, 2002, Hyakutake *et al.*, 2005, Selvaraj *et al.*, 2015). In addition, CheY4 can't bind to FliM because it lacks appropriate interacting residues (Dasgupta & Dattagupta, 2008, Biswas *et al.*, 2013).

*Vc*Aer2 is predicted to be a soluble receptor containing a kinase control module with 51% homology to *Pa*Aer2, three potential methylation sites (EEE), and a C-terminal pentapeptide sequence (EWEEF) for binding adaptation enzymes like CheB3 and CheR3 (Fig. 1B). The principal difference between *Vc*Aer2 and *Pa*Aer2 is that *Vc*Aer2 is predicted to contain two, rather than one, N-terminal PAS (Per-ARNT-Sim) domains: PAS1 (res. 38–157) and PAS2 (res. 165–282) (Fig. 1B). PAS1 is situated in place of the three N-terminal HAMP domains of *Pa*Aer2, whereas PAS2 is positionally equivalent to the *Pa*Aer2 PAS sensing domain, *Pa*PAS (Airola *et al.*, 2010, Watts *et al.*, 2011). By analogy to *Pa*PAS, PAS2 may have a similar sensory role. PAS domains are common sensing and signaling domains in nature that maintain high structural conservation, even in instances of low sequence similarity. This conserved structure consists of an antiparallel β-sheet (containing strands Aβ, Bβ, Gβ, Hβ, and Iβ) surrounded by several α-helices (Cα, Dα, Eα, and Fα) (Moglich *et al.*, 2009). Resolved structures of the *Pa*PAS domain revealed several variations on the conserved PAS theme, including an extended Cα/Dα helix and a short 3_{10} helix called Eη that replaces Eα (Sawai *et al.*, 2012, Airola *et al.*, 2013a). *Pa*PAS binds penta-coordinate *b*-type heme via a His residue on Eη and functions as an O_2 sensor (Garcia *et al.*, 2017). Gas binding displaces a Leu residue on Hβ that occupies the ligand-binding site, causing an unorthodox Trp residue on Iβ to rotate ~90° to stabilize gas binding and initiate signaling (Airola *et al.*, 2013a, Garcia *et al.*, 2017). *Pa*PAS shares 32% and 35% sequence identity with *V. cholerae* PAS1 and PAS2, respectively, whereas PAS1 and PAS2 share 38% sequence identity between themselves. However, both PAS1 and PAS2 contain Eη His residues that should support heme binding and Iβ Trp residues that should stabilize O_2-binding (see Fig. 3A). The purpose of the current study is to gain greater insight into the function and role of Aer2-type chemoreceptors from different microorganisms with a different number of PAS domains. Since Aer2 receptors are likely to be the sole chemoreceptor holding their associated chemosensory clusters together [as is the case for *Pa*Aer2, (Guvener *et al.*, 2006)], this may also shed light on the function of cluster III in *V. cholerae*.

RESULTS

V. cholerae Aer2 can hijack *E. coli* chemotaxis and mediate signaling in response to O_2

The Aer2 ortholog from *P. aeruginosa* (*Pa*Aer2) does not direct chemotaxis in its native host but it can hijack the *E. coli* chemotaxis system and induce ~98% of cells to tumble (a repellent response) in the presence of O_2, CO or NO (Watts *et al.*, 2011). To determine if *V. cholerae* Aer2 (*Vc*Aer2) can similarly elicit *E. coli* responses, *aer2* (VCA1092) was cloned from *V. cholerae* O1 JBK 70 genomic DNA and expressed from pProEXHTa in chemoreceptor-less *E. coli* BT3388, which is smooth biased (~2% tumbling). In *E. coli*, full-length *Vc*Aer2 (res. 1–678, 77.7 kDa including the His-tag) was stable (Fig. 2A) and soluble; it partitioned into the high-speed supernatant after spinning low-speed culture supernatants at 485 000 *g* for 1 hr. When *Vc*Aer2 was expressed in BT3388 under the same

conditions previously used for *Pa*Aer2-mediated responses (200 μM IPTG induction for 45 min), it did not promote cell tumbling in air (20.9% O_2). Induction with 1 mM IPTG for 45 min similarly did not elicit cell tumbling. *Vc*Aer2/BT3388 responses were not observed until cells had been induced with 200 μM IPTG for 2 hr. Under these conditions, ~30% of *Vc*Aer2/BT3388 cells tumbled in air. Adding 25 μg ml^{-1} of 5-aminolevulinic acid (ALA) during growth to accelerate heme synthesis increased the air tumbling response from ~30% to ~50% (Fig. S1A). Ten seconds after air was replaced with N_2, the cells became smooth swimming (~2% of cells tumbled at any time, Fig. S1A). Removing the predicted PAS1 domain from *Vc*Aer2 (*Vc*Aer2 [165–678]) increased receptor stability (Figs. 2A and S2A), but abolished the O_2 response. BT3388 cells expressing *Vc*Aer2 [165–678] swam smoothly and were non-responsive (signal-off) in both air and N_2 (~2% of cells tumbled). Lastly we tested cells expressing full-length *Vc*Aer2 (induced with 200 μM or 1 mM IPTG, and with or without 25 μg ml^{-1} ALA) for a response to CO and NO. *Vc*Aer2-expressing cells did not respond to either CO or NO, unlike BT3388 cells expressing *Pa*Aer2 (Watts *et al.*, 2011).

*Vc*Aer2/BT3388 cells had a repellent response to O_2, and would therefore not be expected to exhibit aerotaxis in tryptone soft agar. When *Vc*Aer2/BT3388 cells were inoculated into tryptone soft agar, they did not elicit either aerotaxis or chemotaxis (with 0 to 1000 μM IPTG, and with or without 25 μg ml^{-1} ALA, Fig. 2B). However, *Vc*Aer2 did inhibit wild-type (WT) *E. coli* RP437 chemotaxis rings in tryptone soft agar after induction with at least 100 μM IPTG (Fig. 2B, 0 and 200 μM IPTG plates are shown). At the same induction levels, PAS1-less *Vc*Aer2 [165–678] also inhibited *E. coli* RP437 chemotaxis (Fig. 2B). Since BT3388 cells expressing *Vc*Aer2 [165–678] are smooth swimming, this inhibition of *E. coli* chemotaxis most likely results from titrating chemotaxis components away from native *E. coli* chemoreceptors.

The PAS1 and PAS2 domains of *Vc*Aer2 both bind *b*-type heme

*Vc*Aer2 contains two predicted PAS domains, PAS1 (res. 38–157) and PAS2 (res. 165–282) (Fig. 1B), which share ~30% sequence identity with *Pa*PAS. PAS1 and PAS2 also have the Eη His that coordinates heme in *Pa*PAS and the Iβ Trp that stabilizes O_2 binding to *Pa*PAS (Fig. 3A). When PAS1 [38–157] and PAS2 [165–282] were expressed in *E. coli* BT3388, both formed stable soluble peptides (Fig. S2C) that purified to ~98% apparent homogeneity on nickel-nitrilotriacetic acid (Ni-NTA) agarose (Fig. 3B). PAS1 and PAS2 both bound *b*-type heme and exhibited spectra similar to *Pa*PAS [Fig. 3C, (Watts *et al.*, 2011)]. In the deoxy-state, both PAS domains had penta-coordinate heme, judged by both a red-shifted Soret peak and a single broad band replacing the α/β-bands of ligand-bound PAS (Fig. 3C). O_2 titrations yielded O_2 dissociation constants [$K_{d(O2)}$] of 12 and 19 μM for PAS1 and PAS2, respectively, while CO titrations gave $K_{d(CO)}$'s of 7 and 5 μM, respectively (see Fig. S3A and C for representative O_2 titrations). These affinities are similar to those previously determined for *Pa*PAS [$K_{d(O2)}$ of 16 μM and $K_{d(CO)}$ of 2 μM, (Garcia *et al.*, 2017)]. In addition, the O_2 and CO affinities of PAS2 were not altered by the presence of the C-terminus in *Vc*Aer2 [165–678] ($K_{d(O2)}$ of 20 μM and $K_{d(CO)}$ of 2 μM). This indicates that the C-terminal HAMP and kinase control domains do not contribute to, or attenuate, gas-binding to PAS2.

Using size exclusion chromatography, the isolated *Pa*PAS domain was determined to be a compact monomer in both its met and deoxy heme states (Watts *et al.*, 2011). In contrast, both *V. cholerae* PAS1 [38–157] and PAS2 [165–282] eluted as homodimers from the same TSKgel G2000SW column in their met heme state (Fig 3D, Mw_{app} of 30 and 33 kDa, respectively) and as more compact homodimers in their deoxy heme state (each with a Mw_{app} of 25 kDa). For PAS 1–2 [1–282] and PAS1 [1–164] peptides, both dimers (Mw_{app} of 75 and 43 kDa, respectively) and larger complexes (Mw_{app} of >200 kDa) were evident, suggesting that the N-terminal 37 amino acids contiguous to PAS1 promote protein aggregation (data not shown).

The Eη His coordinates heme in PAS1 and PAS2

PAS domains often coordinate *b*-type heme via a His residue on Fα (Gilles-Gonzalez & Gonzalez, 2005, Kerby *et al.*, 2008), whereas *Pa*Aer2 coordinates heme via a His residue on Eη (Sawai *et al.*, 2012, Airola *et al.*, 2013a, Garcia *et al.*, 2017). The Eη and Fα His residues are conserved in *Pa*PAS and both *Vc*Aer2 PAS domains (Figs. 3A and 4A). To test the contributions of each His to heme binding and function in PAS1 and PAS2, Eη, Fα, and Eη/Fα His to Ala mutants were created for PAS1 and PAS2 in both PAS peptides and full-length *Vc*Aer2. Similar to what was observed with *Pa*PAS (Garcia *et al.*, 2017), the Eη His mutants (PAS1-H101A and PAS2-H226A) showed substantial heme-binding defects (26% and 2% of WT PAS heme content, respectively), whereas the Fα His mutants (PAS1-H106A and PAS2-H231A) retained WT heme content (Fig. 4B). This confirms that the Eη His coordinates heme in both PAS1 and PAS2. However, 26% of PAS1-H101A molecules retained heme, whereas the dual His mutant PAS1-H101A/H106A retained only 10% heme ($P < 0.05$, Fig. 4B). This phenomenon was also observed for *Pa*PAS (Garcia *et al.*, 2017), and suggests that for PAS1, Fα-H106 may contribute to heme coordination in the absence of Eη-H101. Another possibility is that heme is retained in PAS1-H101A by hydrophobic interactions, and that the additional H106A replacement distorts the heme pocket to impact heme retention. The same conclusions could not be reached for PAS2 because the Eη His mutant, PAS2-H226A, retained only 2% heme.

To determine the effects of the His substitutions on *Vc*Aer2 function, the relevant mutations were introduced into pProEXHTa containing full-length *Vcaer2*. Each of the mutants had steady-state expression levels comparable with WT *Vc*Aer2 (Fig. S2A). In BT3388, the Fα His mutants *Vc*Aer2-H106A and *Vc*Aer2-H231A had WT responses (Fig. S1A). In contrast, *Vc*Aer2-H101A, whose PAS1 peptide retained 26% heme, had a more robust O_2 response than did WT receptor, promoting ~95% cell tumbling in air compared with ~50% tumbling for WT *Vc*Aer2 (Fig. S1E). This response represents the aggregate output of both heme-bound and unbound receptors, but suggests that PAS1 may not be required for O_2 sensing and instead functions to regulate O_2-mediated signaling from PAS2. *Vc*Aer2-H226A, whose PAS2 peptide retained 2% heme, was signal-off biased, directing ~10% of BT3388 cells to tumble in air (Fig. S1C). All of the His mutants tested had WT smooth-swimming responses in response to O_2 removal.

Heme binding requires the entire PAS1 core, but Aer2 function requires the PAS N-cap

PAS domain function often requires a short region N-terminal to the PAS core, called the PAS N-terminal cap (N-cap) (Kurokawa *et al.*, 2004, Watts *et al.*, 2006, Key *et al.*, 2007). N-cap regions contain an Aα′ helix (res. 38–45 in PAS1) and a short loop that precedes the Aβ strand (Aβ begins the PAS1 core at res. 50, Fig. 3A). Both *Pa*PAS structures contain part (Sawai *et al.*, 2012) or all (Airola *et al.*, 2013a) of the Aα′ helix, and heme is bound to the PAS core in both instances. To determine how much of the N-terminus is required for heme binding to PAS1, a series of N-terminal truncations were introduced into *Vc*Aer2-H226A [1–282] (Fig. 5A), and heme content was measured. H226A should prevent ~98% of heme binding to PAS2 (Fig. 4B), so that the heme content of *Vc*Aer2-H226A [1–282] (which contains both PAS1 and PAS2) should instead reflect the amount of heme bound to PAS1. Indeed, the amount of heme bound to *Vc*Aer2-H226A [1–282] was not significantly different from the amount of heme bound to PAS1 [38–157] alone ($P = 0.3$, Fig. 5B, left panel). The heme content of WT *Vc*Aer2 [1–282] was less than twice the heme content of *Vc*Aer2-H226A [1–282], PAS1 [38–157] or PAS2 [165–282] (Fig. 5B, left panel). This discrepancy suggests that it may be more difficult to incorporate two heme molecules into PAS1–2 than incorporate one heme molecule into either PAS1 or PAS2.

Of the N-terminal truncation peptides, only *Vc*Aer2-H226A [38–282] and *Vc*Aer2-H226A [47–282] retained heme; here the heme content matched that of *Vc*Aer2-H226A [1–282] (Figs. 5B and C). Longer truncations abolished any measureable heme (Fig. 5B), even though the corresponding peptides were stably expressed (Fig. S2B). *Vc*Aer2-H226A [57–282], which lacked the PAS1 Aβ strand, contained the shortest truncation that eliminated heme binding (Figs. 5B and C). The N-cap was not required for heme binding, but it was required for function: *Vc*Aer2 [47–678] (with the N-cap removed) and all longer N-terminal truncations resulted in non-functional, signal-off mutants (Fig. 5B). In contrast, *Vc*Aer2 [38–678], which lacked the region N-terminal to the Aα′ helix, had a more robust O_2 response than WT *Vc*Aer2 [1–678] (Figs. 5B and S1E). This finding suggests that the first 37 residues of *Vc*Aer2 are not necessary for Aer2 signaling, but that they assist PAS1 in regulating PAS2 signaling.

The conserved Iβ Trp stabilizes O_2 binding to PAS2 whereas PAS1 uses either the Iβ Trp or a Gβ Tyr residue

In *Pa*PAS, gas binding causes the Iβ Trp, W283, to rotate towards the ligand to stabilize gas binding and initiate signaling (Airola *et al.*, 2013a, Garcia *et al.*, 2017). This may be a canonical mechanism for O_2-signaling in Aer2-type PAS domains, as the Iβ Trp is universally present (Garcia *et al.*, 2017). In *Vc*Aer2, the Iβ Trp resides at W151 in PAS1 (Fig. 6A) and at W276 in PAS2 (Fig. 3A). Of these two PAS domains, PAS2 most closely resembles *Pa*PAS in that it lies directly upstream of the C-terminal HAMP and kinase control domains of *Vc*Aer2 (Fig. 1B). However, in most other chemoreceptors and histidine kinases with tandem PAS-like domains, the second domain does not bind ligands (Zhang & Hendrickson, 2010, Glekas *et al.*, 2012, Nishiyama *et al.*, 2012, Liu *et al.*, 2015, Nishiyama *et al.*, 2016). A notable exception was recently described for the *Helicobacter pylori* TlpC receptor, where the first PAS-like domain binds ligand (Machuca *et al.*, 2017). To determine whether W276 is required for O_2-mediated signaling in PAS2, W276C, F, L and V [selected

because the equivalent *Pa*PAS substitutions retained heme, (Garcia *et al.*, 2017)] were introduced into full-length *Vc*Aer2 and into the PAS2 [165–282] peptide. The mutants were then tested for their responses to, and affinities for, O_2. Similar to *Pa*Aer2-W283L, *Vc*Aer2-W276L was a signal-on biased mutant that caused ~98% of BT3388 cells to tumble in air and had a 30 sec delayed smooth-swimming response in N_2 (Figs. 6B and S1D). Like *Pa*Aer2-W283V, *Vc*Aer2-W276V was signal-off, whereas *Vc*Aer2-W276C was signal-off biased (~20% of cells tumbled in the presence of O_2, Fig. S1C). Purified PAS2 peptides containing W276C, L and V retained heme (Fig. 6C) and bound CO, but none bound O_2 (Fig. 6D). Instead, O_2 rapidly oxidized each peptide from Fe(II) to Fe(III) heme (Fig. S3D), as was previously observed for *Pa*PAS-W283C, L and V (Garcia *et al.*, 2017). Thus, the isolated PAS2-W276L and PAS2-W276C peptides did not stably bind O_2, even though the corresponding full-length receptors responded to O_2 in vivo. This suggests that O_2 binding is too transient to observe in vitro, but is sufficiently stable in vivo to generate partial behavioral responses. A similar scenario was observed for *Pa*Aer2-W283L (Garcia *et al.*, 2017).

In contrast to the other W276 mutants, *Vc*Aer2-W276F was a signal-on biased mutant that retained heme (Figs. 6C and S1D), and bound O_2 and CO with similar affinities to the WT PAS2 domain (Fig. 6D). The same finding was previously observed for *Pa*Aer2-W283F, which was the only Iβ Trp mutant that retained O_2 binding in *Pa*Aer2 (Garcia *et al.*, 2017). Overall, the PAS2-W276 mutants in this study produced comparable results to the corresponding *Pa*PAS-W283 mutants, supporting the hypothesis that the PAS2 Iβ Trp (W276) stabilizes O_2 binding in an analogous manner to *Pa*PAS (W283).

To analyze the PAS1 domain, W151L was introduced into full-length *Vc*Aer2 and into the PAS1 [38–157] peptide and tested for its response to, and affinity for, O_2. Unlike PAS2 and *Pa*PAS, PAS1-W151L bound O_2 and CO with WT affinities (Figs. 6D and S3B). In BT3388, *Vc*Aer2-W151L was a signal-off biased mutant that induced ~10% cell tumbling in air, and ceased tumbling in response to O_2 removal like WT receptor (Figs. 6B and S1C). To determine if O_2 binding was unique to PAS1-W151L, an additional 10 W151 mutants were created by site-directed random or specific mutagenesis. PAS1 [38–157] peptides containing W151E, W151N and W151R, had low heme binding (9–13% of WT heme content, Fig. 6C) and gas-binding affinities could not be determined. The seven remaining PAS1-W151 mutants (W151C, F, G, P, S, T and V) had at least 41% heme content compared with WT PAS1 (Fig. 6C) and bound O_2 and CO with WT affinities (Fig. 6D). The corresponding full-length *Vc*Aer2-W151 mutants also responded to O_2 with either signal-off or -on biased, WT or more robust (>WT) behavior (Figs. 6B and S1). Overall, these data suggest that W151 alone does not stabilize O_2 binding to the PAS1 domain.

To find residues other than W151 that might stabilize O_2-binding in the distal heme pocket of PAS1, polar residues within 10 Å of ligand bound heme were sought by comparing the sequence of PAS1 with the structure of *Pa*PAS (Sawai *et al.*, 2012). In the distal heme pocket, only W151, M52 (on Aβ) and Y119 (on Gβ) were potentially within range to contact a ligand bound to heme (Fig. 6A), so we created Leu mutants of M52 and Y119 in full-length *Vc*Aer2. In BT3388, *Vc*Aer2-M52L had a more robust O_2 response than WT, whereas *Vc*Aer2-Y119L was signal-off biased (~25% of cells tumbled in the presence of

O_2, Fig. S1C). Analysis of the PAS1-Y119L peptide showed that it had WT heme content and WT O_2 and CO affinities (Fig. 6). Thus, single residues with the potential to stabilize O_2 were dispensable for O_2 binding to PAS1. We next considered whether a combination of amino acids could provide O_2-stabilizing interactions for PAS1, similar to what has been described for Ascaris hemoglobin [Tyr and Gln, (Yang *et al.*, 1995)] and for soybean leghemoglobin [Tyr and His, (Kundu & Hargrove, 2003)]. We created a PAS1 peptide and full-length *Vc*Aer2 receptor containing dual Y119L and W151L substitutions. In BT3388, *Vc*Aer2-Y119L/W151L did not respond to O_2 (it was signal-off), and PAS1-Y119L/W151L bound heme and CO, but it did not bind O_2 (Fig. 6). This suggests that interactions from either Y119 or W151 stabilize O_2 binding to PAS1.

Signal-on behavior is not dependent on Aer2 methylation

Robust *Pa*Aer2 responses in *E. coli* require Aer2 methylation by *E. coli* CheR (Watts *et al.*, 2011). However, signal-on mutants of *Pa*Aer2 are signal-on irrespective of methylation status (Garcia *et al.*, 2017). To determine if this is also true for *Vc*Aer2 mutants, mutants that were determined to have signal-on biased behavior or more robust signaling responses than WT (Figs. 5B and 6B) were expressed in *E. coli* UU2610, which lacks all *E. coli* chemoreceptors in addition to the adaptation enzymes CheR and CheB. In UU2610, the tumbling biases of cells expressing the three signal-on biased mutants (*Vc*Aer2-W151F, *Vc*Aer2-W276F or *Vc*Aer2-W276L) and the more robust response mutants *Vc*Aer2-W151G and *Vc*Aer2-W151T were unaffected by the lack of *E. coli* adaptation enzymes (Fig. S1F). This suggests that the signaling behavior induced by these receptors is primarily due to the PAS residue substitutions, rather than receptor methylation status. In contrast, the tumbling biases of cells expressing WT *Vc*Aer2, *Vc*Aer2 [38–678], *Vc*Aer2-M52L, *Vc*Aer2-H101A, and *Vc*Aer2-W151S were reduced by 20–40% in air (Fig. S1F), suggesting that methylation partly contributes to the signal-on biases observed for these receptors in air.

The structure of the PAS2 domain

The structure of the signal-on PAS2-W276L peptide with ferric [Fe(III)] heme was determined to 1.67 Å resolution (Table S1, PDB code: 6CEQ). PAS2-W276L maintained a conserved PAS fold with most features similar to those of *Pa*PAS (Fig. 7A–B), including the PAS β-sheet consisting of Aβ, Bβ, Gβ, Hβ and Iβ and the extended Cα/Dα helix with a kink at R201 (A209 in *Pa*PAS). Also like *Pa*PAS, the Eα helix was distorted into an Eη helix. The Eη His residue H226 was 2.5 Å from the Fe atom and, as anticipated, served as the proximal heme ligand (Fig. 7C–D).

Despite the overall similarity between PAS2-W276L and *Pa*PAS, there were also some notable structural differences. Whereas the N-cap of *Pa*PAS forms a well defined Aα′ helix (Sawai *et al.*, 2012, Airola *et al.*, 2013a), that of PAS2-W276L continued the extended structure of the Aβ strand to end in a disordered region (Fig. 7A–B). Indeed, electron density for the first five residues of PAS2-W276L was not discernible. Sequence homology in the Aα′ region is relatively strong between PAS2-W276L and *Pa*PAS, which suggests that other factors, including the W276L substitution and possibly crystal contacts, may influence the conformational difference in the N-cap. PAS2-W276L formed an antiparallel dimer in the crystal with β-β contacts that included the extended Aβ′, whereas *Pa*PAS crystallizes as a

parallel dimer whose subunit interface is formed from both the Aα′ helices and the β-sheets (Airola *et al.*, 2013a). In addition to these differences in conformation and oligomerization, PAS2-W276L also contained an additional turn of 3_{10} helix between the Fα helix and the Gβ strand that is not found in *Pa*PAS.

Both PAS2 and *Pa*PAS bind *b*-type hemes that associate into a hydrophobic pocket of non-polar side chains. For *Pa*PAS, H251 on the Gβ strand hydrogen bonds with the 7-propionate of the heme (Sawai *et al.*, 2012, Airola *et al.*, 2013a). PAS2 contains Phe (F244) instead of His at this position, but in PAS2, H231 is shifted closer to the heme propionate than its counterpart, H239 in *Pa*PAS (Fig. 7C–D) to provide a compensating interaction.

Consequences of Trp substitution in the distal ligand-binding pocket of PAS2

Although PAS2-W276L was crystalized in the ferric, ligand-free form, its overall structure was more similar to the structure of CN^--bound *Pa*PAS than to the structure of unliganded ferric *Pa*PAS. This similarity was especially true at the C-terminal β-strands (Gβ-Hβ-Iβ), which aligned well with those of CN^--bound *Pa*PAS (Fig. 7B). In addition, the PAS2-W276L variant appeared to recapitulate the conformational changes of the CN^--bound species despite having an unoccupied distal pocket (Fig. 7A–D). The substitution of the W276 indole ring for the shorter Leu side chain promoted a similar movement of Gβ-Hβ-Iβ towards the heme carboxylates and the periphery of the protein, including a displaced Hβ Leu (Fig. 7A–D). In PAS2-W276L, these combined motions led to both a shift in the position of the Iβ strand and changes in the interactions between the PAS β-sheet and juxtaposed Aα′, which completely dissociated from the protein core. Importantly, the spatial arrangement of the Iβ strand is critical for signal transduction because it connects directly to the downstream HAMP domains. Furthermore, the Aα′ helix contributes to the proposed PAS-PAS interface in the full-length protein (Sawai *et al.*, 2012, Airola *et al.*, 2013a). Thus, the Iβ Trp indole buttresses the Gβ-Hβ-Iβ region against the porphyrin, and either its substitution to Leu, or reorientation due to ligand binding, elicits similar repositioning of the PAS β-sheet and subsequent repacking of Aα′. The signal-on-biased character of *Vc*Aer2-W276L is thus consistent with the similarity of the PAS2-W276L structure to that of the ligand-bound form of *Pa*PAS.

PAS1 structural model

A homology model was created for the wild type PAS1 domain by threading the PAS1 sequence (res. 38–157) onto the PAS2-W276L structure. The heme-binding pockets of PAS1 and PAS2 showed high similarity for the proximal heme-ligating residue (H101 in PAS1 and H226 in PAS2) and distal ligand-coordinating residue (W151 in PAS1 and W276 in PAS2) (Fig. 7E–F). In both PAS domains the Fα His (H106 in PAS1 and H231 in PAS2) formed a hydrogen bond with the 7-propionate of the heme, as did an Fα Gln (Q107 in PAS1 and Q232 in PAS2) (Fig. 7 E–F). Some minor differences in the distal ligand-binding pocket included the change of F244 to Y119 in PAS1 (which contributes to O_2 binding) and also S246 to T121 (Fig. 7E–F). Interestingly, given this high degree of homology, relatively conservative changes in ionizable residues produce a considerably more negative potential in the heme pocket for PAS1 compared to PAS2 (Fig. S4). The O_2 affinity of heme proteins can depend on many factors including proximal ligand electronic effects, distal ligand

hydrogen bonding, heme distortions and heme redox potential. Lower potential hemes (those in more negative environments) generally produce more stable O_2 binding by favoring the ferric-superoxy state of the heme-liganded complex (Grinstaff *et al.*, 1995). Hence, the more negative heme environment of PAS1 may contribute to stable oxy complexes in the absence of either Y119 or W151.

DISCUSSION

V. cholerae Aer2 is a dual-PAS heme O_2 sensor

In this study we have shown that the *V. cholerae* cluster III chemoreceptor, *Vc*Aer2, directly senses O_2 via two PAS-heme domains. This was shown in vitro by measuring the O_2 binding affinity of each PAS domain, and in vivo in *E. coli* by demonstrating the O_2-directed response of full-length *Vc*Aer2. In *V. cholera*e, cluster III proteins (Fig. 1) do not direct chemotaxis or aerotaxis (Gosink *et al.*, 2002, Hyakutake *et al.*, 2005, Dasgupta & Dattagupta, 2008, Biswas *et al.*, 2013), but when *Vc*Aer2 was expressed in *E. coli*, it orchestrated a repellent response to O_2. The ability to hijack (Fig. 2B) and control *E. coli* chemotaxis presumably stems from the 54% sequence homology between the kinase control module of *Vc*Aer2 (Fig. 1B) and the major *E. coli* chemoreceptor Tsr. When *Vc*Aer2 was expressed in *E. coli* BT3388, the most robust signaling response occurred when ALA, the first compound in the porphyrin synthesis pathway, was added to cultures during growth. This response was weaker than that observed for *Pa*Aer2: ~50% of WT *Vc*Aer2/BT3388 cells tumbled in air (with ALA) compared with ~98% for *Pa*Aer2/BT3388 [without ALA, (Watts *et al.*, 2011)]. Cells ceased tumbling when air was removed, indicating that O_2 had activated *Vc*Aer2 signaling. The lower tumbling bias of *Vc*Aer2/BT3388 versus *Pa*Aer2/BT3388 in air may reflect differences in predicted methylation sites, which, when methylated, promote the kinase-on state. *Vc*Aer2 has three methylation sites (EEE), while *Pa*Aer2 has four (QEEE) including a signal-inducing Gln that is not efficiently deamidated by *E. coli* CheB (Watts *et al.*, 2011). Unlike *Pa*Aer2, *Vc*Aer2 did not respond to CO or NO even though CO bound to both PAS1 and PAS2 (Fig. 3C).

*Vc*Aer2 differs from *Pa*Aer2 in that it has two N-terminal PAS domains (Fig. 1B). PAS1 replaces the HAMP1–3 domains of *Pa*Aer2, and PAS2 is positionally equivalent to *Pa*PAS (Airola *et al.*, 2010, Watts *et al.*, 2011). Our preliminary analysis suggests that this Aer2 architecture also exists in other microbes, e.g., in *Shewanella oneidensis* SO2123, where both predicted PAS domains contain the Eη His and Iβ Trp residues. The Aer2 ortholog from *Vibrio vulnificus* (Mcp III) is predicted to have three PAS domains and each PAS domain contains the conserved Eη His and Iβ Trp residues. In *Vc*Aer2, both PAS1 and PAS2 coordinated *b*-type heme via Eη-His and exhibited spectra and gas-binding affinities that were similar to *Pa*PAS [(Garcia *et al.*, 2017), Figs. 3, 4 and 6]. The O_2 affinities of PAS1 and PAS2 (12 and 19 μM, respectively) were comparable to *Pa*Aer2 (16 μM) and to those of other O_2-sensing PAS domains, e.g., *E. coli* DOS (13 μM) and *Sinorhizobium meliloti* FixL (31 μM) (Delgado-Nixon *et al.*, 2000, Gilles-Gonzalez & Gonzalez, 2005, Garcia *et al.*, 2017). It is probable that Aer2 homologs are all PAS heme-O_2 sensors, regardless of their specific PAS-HAMP domain architecture.

PAS N-cap rearrangements and *Vc*Aer2 signaling

In *Vc*Aer2, the entire PAS core was required for heme binding to PAS1 (Fig. 5). The Aα′ helix of the PAS1 N-cap was not required for heme binding, but it was required for *Vc*Aer2 function (Fig. 5). PAS N-caps are functionally important, and in *Pa*PAS and other PAS dimers, the Aα′ helix, along with the PAS β-sheet, stabilize the PAS dimer interface (Watts *et al.*, 2006, Key *et al.*, 2007, Moglich *et al.*, 2009, Airola *et al.*, 2013a). In solution, the isolated PAS1 and PAS2 peptides formed homodimers in both met heme (Fig. 3D) and deoxy heme states, yet homodimers were more compact in the deoxy, unliganded state. Previously, when the structure of the CN^--bound *Pa*PAS monomer was superimposed on the ligand-free *Pa*PAS dimer structure, collisions occurred between the N-caps and Hβ strands (Airola *et al.*, 2013a). Incompatibility of the ligand-bound form with the ligand-free dimer suggested that ligand binding to the Aer2-PAS domain promotes PAS-PAS rearrangements at the dimer interface that involves the PAS N-cap. In the current study, removing Aα′ from PAS1 resulted in a signal-off phenotype (Fig. 5). This may indicate that PAS1 does not dimerize correctly in the absence of Aα′, and/or that rearrangements of the Aα′ helix are essential for *Vc*Aer2 signaling. In further support of this idea, it is striking that the structure of the PAS2-W276L signal-on variant was very different from that of *Pa*PAS in the region of Aα′ despite strong sequence similarity between the two proteins. The dissociation and unfolding of Aα′ from the PAS2 β-sheet may well promote an activated conformation in keeping with the behavior of this variant. Structural changes in both N-cap and C-cap elements on the opposite side of the β-sheet from the ligand-binding pocket is a common feature of PAS domain signaling. A classic example involves restructuring of the Jα and Aα′ helices in LOV domain proteins (Harper *et al.*, 2003, Zoltowski *et al.*, 2007). The fact that the signal-on variant of PAS2 had a completely dissociated Aα′ helix is in keeping with this theme. The antiparallel dimer formed in the crystal of PAS2-W276L is likely only a consequence of favorable packing for this altered conformation, but the change in conformation for Aα′ is a strong indication that perturbations in the ligand-binding pocket are relayed through changes in the Hβ-Gβ-Iβ strands, where they are able to alter the conformation and thereby interactions of the N-cap. The structure of PAS2-W276L supports the view that ligand binding ultimately restructures the PAS-PAS interface in full-length Aer2 proteins.

The distinct roles of the PAS1 and PAS2 domains of *Vc*Aer2

The PAS1 and PAS2 domains of *Vc*Aer2 both bound O_2 with similar affinities (Fig. 6D), but they stabilized O_2 binding by different mechanisms. In PAS2, the Iβ Trp, W276, stabilized O_2 binding in an analogous manner to the Iβ Trp, W283, from *Pa*Aer2 (Garcia *et al.*, 2017). PAS2 peptides containing W276C, L and V were rapidly oxidized by O_2 (Fig. S3D), whereas W276F bound O_2 with WT affinity (Fig. 6D). This finding is similar to that of *Pa*Aer2, where W283F was the only Iβ Trp mutant that retained O_2 binding. In that case O_2 stabilization may have occurred via a solvent molecule in a manner similar to that shown for a Tyr to Phe replacement mutant of *Mycobacterium tuberculosis* DevS (Yukl *et al.*, 2008). PAS1 was different; the Iβ Trp mutants PAS1-W151C, F, G, L, P, S, T and V all bound O_2 with WT affinities (Fig. 6D), and their corresponding full-length mutants responded to O_2 (Figs. 6B and S1). For PAS O_2 sensors that bind *b*-type heme, only the Iβ Trp residue (in Aer2) and a Gβ Arg residue [in FixL, DOS and PDEA-1 (Gilles-Gonzalez

& Gonzalez, 2005)] have been shown to H-bond to ligand in the distal heme pocket. In other heme proteins, His [e.g., vertebrate hemoglobin and myoglobin], Gln and Tyr [e.g., Ascaris hemoglobin (Kloek *et al.*, 1994)] stabilize O_2 binding. In soybean leghemoglobin, a combination of His and Tyr residues synergistically provide weak interactions with bound O_2 (Kundu & Hargrove, 2003). The proximal heme pocket of leghemoglobin enhances Fe^{2+}-O_2 interactions and the weak distal pocket interactions facilitate faster O_2 dissociation. In *Vc*Aer2, PAS1-Y119L and PAS1-W151L both had WT O_2 and CO affinities, whereas PAS1-Y119L/W151L bound CO, but did not bind O_2 (Fig. 6D). In leghemoglobin, removal of either the His or Tyr residues allowed the remaining side-chain to stabilize O_2 to a larger extent than both in combination (Kundu & Hargrove, 2003). A similar scenario in *Vc*Aer2 might explain why the O_2 affinity of PAS1 was not affected by individually removing Y119 or W151. Whether PAS1, like leghemoglobin, requires faster O_2 dissociation is currently under investigation.

In *Pa*PAS, gas binding displaces the Hβ Leu that occupies the ligand-binding site, eliciting the Iβ Trp to rotate towards the ligand. These movements stabilize gas binding and initiate conformational signaling (Airola *et al.*, 2013a, Garcia *et al.*, 2017). The Hβ Leu is also conserved in PAS1 and PAS2 (Fig. 3A) and presumably moves out of the ligand-binding site for O_2 binding in both PAS domains. It is intriguing that the signal-on mutant W276L assumed an activated conformation with the Hβ Leu displaced in the absence of ligand. This finding suggests that, although the distal Hβ Leu must certainly move for the heme to bind ligand, ligand-induced rearrangements of the Iβ Trp may be the dominant factor in promoting the switch to the active conformation.

In most chemoreceptors or histidine kinases with tandem PAS-like domains, the second domain does not bind small ligands (Nishiyama *et al.*, 2016, Machuca *et al.*, 2017). This is clearly not the case for *Vc*Aer2, where PAS2 binds O_2 and signals its binding. Our data suggest that the primary role of PAS1 is to regulate O_2-mediated signaling from PAS2. For example, *Vc*Aer2-H101A, whose PAS1 peptide retained only 26% heme (Fig. 4B), had a more robust O_2 response than did WT receptor. An additional four PAS1 mutants likewise had better than WT function (Figs. 6B and S1E). However, removing PAS1 altogether (*Vc*Aer2 [165–678]) resulted in a non-functional receptor, even though PAS2 presumably remained dimeric. The only PAS1 mutant in this study that did not bind O_2 (PAS1-Y119L/W151L) was similarly non-functional. Thus, PAS1-heme appears tuned to regulate PAS2 function, and this function may require PAS1 to bind O_2. Since the Iβ strand of PAS1 is fused directly to the N-cap of PAS2, regulatory effects could be directed through the PAS1 Iβ-PAS2 N-cap connection, or could involve more global changes, such as PAS domain rotations or association/dissociation (signal-off, deoxy heme/signal-on, ligand bound heme, respectively). PAS2-mediated signaling then results in activation of the cluster III chemosensory pathway (Fig. 1B), resulting in a cellular response.

EXPERIMENTAL PROCEDURES

Mutagenesis and cloning

The *aer2* gene (VCA1092) was amplified from *V. cholerae* O1 JBK 70 (Kaper *et al.*, 1984) genomic DNA using PfuUltra DNA polymerase (Agilent Technologies, Santa Clara,

CA) and cloned into the NcoI and PstI sites of pProEXHTa to express *Vc*Aer2 (res. 1–678) with an N-terminal His_6 tag. This construct was named pKGB1. To create PAS peptides or *Vc*Aer2 constructs with N-terminal truncations, DNA fragments were PCR amplified from pKGB1, pKGB1-derived plasmids, or from *V. cholerae* O1 JBK 70 genomic DNA and cloned into the NcoI and PstI sites of pProEXHTa or the NdeI and XhoI sites of pET28a. Site-directed mutagenesis was performed on pKGB1, pProEXHTa-PAS2 (for PAS2-W276F), or pET28a-PAS2 (for PAS2-W276L) using site-specific primers and PfuUltra II Fusion DNA polymerase (Agilent Technologies) or Phusion® DNA polymerase (New England Biolabs, Ipswich, MA). For site-directed random mutagenesis, primers containing an equimolar mix of all four nucleotides at the W151 codon were used to amplify pKGB1 with 66 °C annealing and 20 amplification cycles. Site-specific mutagenesis products were treated with DpnI (New England Biolabs) to remove template strands and then electroporated into *E. coli*. For all constructs, *Vc*Aer2 expression was induced with 600 μM IPTG and products of the correct size were confirmed by Western blotting with HisProbe™-HRP (Thermo Scientific, Rockford, IL). All protein masses in this manuscript are reported for proteins without heme. All mutations were confirmed by sequencing the entire *aer2* coding sequence.

Bacterial strains

*Vc*Aer2 plasmids were expressed in *E. coli* BL21(DE3), the WT *E. coli* chemotaxis strain RP437 (Parkinson, 1978), and in the chemoreceptorless *E. coli* strains BT3388 [*tar, tsr, trg, tap, aer* (Yu *et al.*, 2002)] and UU2610 [*tar, tsr, trg, tap, aer, cheR, cheB* (Zhou *et al.*, 2011)].

Steady-state cellular *Vc*Aer2 levels

The steady-state cellular levels of the full-length *Vc*Aer2 mutants (res. 1–678) and N-terminal truncation mutants were compared with WT *Vc*Aer2 after inducing BT3388 cells with 50 μM IPTG (Fig. S2A). Aer2-W151E and Aer2-W151R were instead induced with 200 μM IPTG. The cellular levels of the PAS peptides were compared with PAS1–2 (res. 1–282, with or without H226A, Fig. S2B–C), WT PAS1 (res. 38–157, Fig. S2D), or WT PAS2 (res. 165–282, Fig. S2E) after inducing expression in BT3388 with 100 μM IPTG. PAS1-W151E, PAS1-W151N, and PAS1-W151R were instead induced with 200 μM IPTG. Samples were electrophoresed in duplicate and experiments were repeated on two to four separate occasions. Bands were visualized on HisProbe Western blots and quantified on a BioSpectrum® digital imager (UVP, Upland, CA).

Behavioral assays

BT3388 cells were grown at 30 °C in tryptone broth containing 0.5 μg ml^{-1} thiamine and 25 μg ml^{-1} 5-aminolevulinic acid (Sigma-Aldrich) and induced at an OD_{600nm} of 0.2–0.25 for 2 h with 200 μM IPTG. Cells were then placed in a gas perfusion chamber where the gas was toggled between air (20.9% O_2) and N_2, and cell behavior was analyzed (Rebbapragada *et al.*, 1997, Taylor *et al.*, 2007). Signal-off mutants (those that were smooth swimming in air and in N_2) were retested after inducing expression with 1 mM IPTG for 2 h. Behavioral responses to O_2 were repeated two or more times on at least two separate occasions. Estimation of percent tumbling was determined for all motile bacteria in a field of view at 800× magnification. To determine CO responses, BT3388 cells induced with 200 μM or 1

mM IPTG were perfused with N_2 for 30 sec prior to perfusing with CO gas (>99% purity, Sigma-Aldrich, St. Louis, MO) for 10 sec. NO responses were assessed using the NO donor Proli NONOate as previously described (Watts *et al.*, 2011). Swim plate responses were determined by inoculating RP437 or BT3388 cells into tryptone soft agar containing 0–1000 μM IPTG (Taylor *et al.*, 2007) and incubating at 30 °C for 9–16 h.

Protein purification for heme and gas binding studies

BT3388 cells expressing full-length *Vc*Aer2, truncation mutants or PAS peptides were grown in LB broth, Lennox (5 g L^{-1} NaCl), containing 0.5 μg ml^{-1} thiamine and 25 μg ml^{-1} 5-aminolevulinic acid to augment heme synthesis and incorporation. Protein expression was induced with 600 μM IPTG and proteins were purified on Ni-NTA agarose columns (Qiagen, Valencia, CA) as previously described (Garcia *et al.*, 2017). In addition to wash buffers 1 and 2 (containing 50 mM Tris, pH 7.5, 100 mM NaCl and 20 mM or 50 mM imidazole, respectively), all PAS peptides except PAS2 peptides were also washed with wash buffer 3 (containing 100 mM imidazole). The concentration of the eluted proteins was determined in a BCA™ Protein Assay (Thermo Scientific) using BSA as a standard, and sample quality was assessed by SDS-PAGE (2.5 μg of each protein), followed by staining with Coomassie Brilliant Blue.

Heme binding

The proportion of heme bound to the WT PAS1 (res. 38–157) and PAS2 (res. 165–282) peptides was determined by using a pyridine hemochrome assay (Garcia *et al.*, 2017). Results were used to standardize PAS-heme concentrations in ligand-binding assays. To determine the heme content of purified PAS peptides, the Soret height and purity of 10 μM imidazole-bound PAS peptides were compared with corresponding WT PAS peptides, as previously described (Garcia *et al.*, 2017). Full-length *Vc*Aer2 and *Vc*Aer2 [165–678] were analyzed using 5 μM purified protein. Heme ratios below 15% indicated a substantial heme-binding defect from which gas affinity constants could not be determined.

Absorption spectra and gas binding affinities

The deoxy, oxy, carbonmonoxy and met heme spectra of 10 μM purified PAS1 (res. 38–157) and PAS2 (res. 165–282) were determined as previously described for *Pa*Aer2 (Watts *et al.*, 2011). Dissociation constants for O_2 ($K_{d(O2)}$) and CO ($K_{d(CO)}$) binding to PAS1, PAS2 and *Vc*Aer2 [165–678] peptides were estimated by linear interpolation of unliganded (Fe^{2+}) and liganded (Fe^{2+}-O_2, Fe^{2+}-CO) spectra, as previously described (Garcia *et al.*, 2017). Experiments were repeated on two to eight occasions, from which average K_d's were determined and rounded to the nearest whole number.

Solubility assays

*Vc*Aer2/BT3388 cells were grown, lysed and centrifuged at low (10 000 *g*) and then high (485 000 *g*) speed as per the protein purification method above. Low- and high-speed pellets were resuspended in buffer containing 50 mM Tris, pH 7.5, 100 mM NaCl and 10 mM imidazole. Equal volumes of the low- and high-speed supernatants and resuspended pellets were analyzed by SDS-PAGE and HisProbe Western blots.

Size-exclusion chromatography

Purified PAS peptides and protein standards [from Schwarz/Mann Biotech (Cleveland, OH) and Sigma-Aldrich] were filtered though 0.2 μM centrifugal filters (Millipore, Billerica, MA) and 200 μg of proteins (in 100 μl) were separated on a TSKgel G2000SW size-exclusion column (Tosoh Bioscience, King of Prussia, PA) in 50 mM $NaPO_4$, pH 7.0, 300 mM NaCl and 0.02% NaN_3 (TSK buffer), as previously described (Watts *et al.*, 2011). Under these conditions, imidazole dissociated from the PAS peptides, leaving met heme. To analyze peptides containing deoxy heme, TSK buffer was perfused with N_2 for at least one hour, before adding sodium dithionite to 2 mM and perfusing with N_2 for an additional 15 min. The column was then equilibrated with this buffer for 15 min. Sodium dithionite grains were added to the protein samples before loading onto the column. The presence of deoxy heme was determined by monitoring the elution spectra. For all samples, 1 ml fractions were collected and analyzed after ammonium sulfate precipitation for the presence of PAS peptide on HisProbe Western blots.

Crystallization and data collection

PAS2-W276L was expressed in *E. coli* BL21(DE3) along with *E. coli* ferrochelatase to promote PAS-heme incorporation (Sudhamsu *et al.*, 2010). Protein expression was induced with 400 μM IPTG at 37 °C for 16 hours. PAS2-W276L was purified on a Ni-NTA column and eluted in 10 mM Tris pH 8.0, 500 mM NaCl, 10% glycerol and 250 mM Imidazole pH 8.0. The eluted peptide was subjected to buffer exchange into 20 mM imidazole pH 8.0 and 100 mM NaCl before overnight digestion with thrombin (0.7 μg ml^{-1}). The tag-free peptide was further purified using a Superdex 75 26–60 size exclusion column (GE Life Sciences, Pittsburgh, PA), and eluted in 20 mM imidazole pH 8.0 and 100 mM NaCl. Crystals of PAS2-W276L were grown by vapor diffusion upon mixing 1 μl of protein (12 mg ml^{-1}) with 1 μl of well solution against a reservoir containing 2.6 M $(NH_4)_2SO_4$, 0.1 M citric acid pH 5.5. A solution of $NiCl_2$ (10 mM final concentration) was added directly to the protein-well solution mixture to influence crystallization and promote better diffraction. Diffraction data was collected at the Cornell High Energy Synchroton Source (CHESS) on the A1 beamline with an ADSC Quantum 210 CCD detector. Data were processed with HKL2000 (Otwinowski & Minor, 1997).

Structure determination and refinement

The structure of PAS2-W276L in the ligand-free form was determined by molecular replacement with PHENIX AutoMR using the CN^--bound *Pa*PAS structure (PDB code: 3VOL) as a search model. The structure was built using Coot (Emsley *et al.*, 2010), and refined in PHENIX (Adams *et al.*, 2011) amid manual model building, minimization, *B*-factor refinement, and application of non-crystallographic symmetry (NCS) restraints. NCS restraints were removed in the later stages of refinement.

Homology modelling

Homology models of WT PAS1 (res. 38–157) and WT PAS2 were produced based on the PAS2-W276L structure using SWISS-MODEL (Arnold *et al.*, 2006). A *b*-type heme molecule was positioned into the PAS1 homology model by superimposing the heme-

containing PAS2-W276L structure. The same heme-ligation pattern was maintained as found in the PAS2-W276L structure.

Supplementary Material

Refer to Web version on PubMed Central for supplementary material.

Acknowledgments

We thank Kahryl Bennett, Adwoa Wiafe, Andrew Hong, Magi Ishak Gabra, and Lana Haddad for constructing and testing several of the mutants in this study. This research was supported by laboratory start-up funds to K. Watts, the Loma Linda University Center for Health Disparities and Molecular Medicine (CHDMM) summer research program [National Institutes of Health (NIH) award number P20MD006988], the National Institute of General Medical Sciences (NIGMS) of the NIH award number R01GM108655 to K. Watts, and award number R35GM122535 to B. Crane. The content is solely the responsibility of the authors and does not represent the official views of the National Institutes of Health.

References

Adams PD, Afonine PV, Bunkoczi G, Chen VB, Echols N, Headd JJ, Hung LW, Jain S, Kapral GJ, Kunstleve RWG, McCoy AJ, Moriarty NW, Oeffner RD, Read RJ, Richardson DC, Richardson JS, Terwilliger TC, Zwart PH. 2011; The Phenix software for automated determination of macromolecular structures. Methods. 55: 94–106. [PubMed: 21821126]

Airola MV, Huh D, Sukomon N, Widom J, Sircar R, Borbat PP, Freed JH, Watts KJ, Crane BR. 2013a; Architecture of the soluble receptor Aer2 indicates an in-line mechanism for PAS and HAMP domain signaling. J Mol Biol. 425: 886–901. [PubMed: 23274111]

Airola MV, Sukomon N, Samanta D, Borbat PP, Freed JH, Watts KJ, Crane BR. 2013b; HAMP domain conformers that propagate opposite signals in bacterial chemoreceptors. PLOS Biol. 11: e1001479. [PubMed: 23424282]

Airola MV, Watts KJ, Bilwes AM, Crane BR. 2010; Structure of concatenated HAMP domains provides a mechanism for signal transduction. Structure. 18: 436–448. [PubMed: 20399181]

Arnold K, Bordoli L, Kopp J, Schwede T. 2006; The SWISS-MODEL workspace: a web-based environment for protein structure homology modelling. Bioinformatics. 22: 195–201. [PubMed: 16301204]

Biswas M, Dey S, Khamrui S, Sen U, Dasgupta J. 2013; Conformational barrier of CheY3 and inability of CheY4 to bind FliM control the flagellar motor action in *Vibrio cholerae*. PLOS One. 8: e73923. [PubMed: 24066084]

Boin MA, Austin MJ, Hase CC. 2004; Chemotaxis in *Vibrio cholerae*. FEMS Microbiol Lett. 239: 1–8. [PubMed: 15451094]

Briegel A, Ortega DR, Mann P, Kjaer A, Ringgaard S, Jensen GJ. 2016; Chemotaxis cluster 1 proteins form cytoplasmic arrays in *Vibrio cholerae* and are stabilized by a double signaling domain receptor DosM. Proc Natl Acad Sci USA. 113: 10412–10417. [PubMed: 27573843]

Dasgupta J, Dattagupta JK. 2008; Structural determinants of *V. cholerae* CheYs that discriminate them in FliM binding: comparative modeling and MD simulation studies. J Biomol Struct Dyn. 25: 495–503. [PubMed: 18282004]

Delgado-Nixon VM, Gonzalez G, Gilles-Gonzalez MA. 2000; Dos, a heme-binding PAS protein from *Escherichia coli*, is a direct oxygen sensor. Biochemistry. 39: 2685–2691. [PubMed: 10704219]

Emsley P, Lohkamp B, Scott WG, Cowtan K. 2010; Features and development of Coot. Acta Crystallogr D Biol Crystallogr. 66: 486–501. [PubMed: 20383002]

Garcia D, Orillard E, Johnson MS, Watts KJ. 2017; Gas sensing and signaling in the PAS-heme domain of the *Pseudomonas aeruginosa* Aer2 receptor. J Bacteriol. 199: 3–17.

Gilles-Gonzalez MA, Gonzalez G. 2005; Heme-based sensors: defining characteristics, recent developments, and regulatory hypotheses. J Inorg Biochem. 99: 1–22. [PubMed: 15598487]

Glekas GD, Mulhern BJ, Kroc A, Duelfer KA, Lei V, Rao CV, Ordal GW. 2012; The Bacillus subtilis chemoreceptor McpC senses multiple ligands using two discrete mechanisms. J Biol Chem. 287: 39412–39418. [PubMed: 23038252]

Gosink KK, Kobayashi R, Kawagishi I, Hase CC. 2002; Analyses of the roles of the three cheA homologs in chemotaxis of *Vibrio cholerae*. J Bacteriol. 184: 1767–1771. [PubMed: 11872729]

Grinstaff MW, Hill MG, Bimbaum ER, P SW, Labinger JA, Gray HB. 1995; Structures, electronic properties, and oxidation-reduction reactivity of halogenated iron porphyrins. Inorg Chem. 34: 4896–4902.

Guvener ZT, Tifrea DF, Harwood CS. 2006; Two different *Pseudomonas aeruginosa* chemosensory signal transduction complexes localize to cell poles and form and remould in stationary phase. Mol Microbiol. 61: 106–118. [PubMed: 16824098]

Harper SM, Neil LC, Gardner KH. 2003; Structural basis of a phototropin light switch. Science. 301: 1541–1544. [PubMed: 12970567]

Hiremath G, Hyakutake A, Yamamoto K, Ebisawa T, Nakamura T, Nishiyama S, Homma M, Kawagishi I. 2015; Hypoxia-induced localization of chemotaxis-related signaling proteins in *Vibrio cholerae*. Mol Microbiol. 95: 780–790. [PubMed: 25420689]

Hyakutake A, Homma M, Austin MJ, Boin MA, Hase CC, Kawagishi I. 2005; Only one of the five CheY homologs in *Vibrio cholerae* directly switches flagellar rotation. J Bacteriol. 187: 8403–8410. [PubMed: 16321945]

Kaper JB, Lockman H, Baldini MM, Levine MM. 1984; Recombinant nontoxinogenic *Vibrio cholerae* strains as attenuated cholera vaccine candidates. Nature. 308: 655–658. [PubMed: 6324005]

Kerby RL, Youn H, Roberts GP. 2008; RcoM: a new single-component transcriptional regulator of CO metabolism in bacteria. J Bacteriol. 190: 3336–3343. [PubMed: 18326575]

Key J, Hefti M, Purcell EB, Moffat K. 2007; Structure of the redox sensor domain of *Azotobacter vinelandii* NifL at atomic resolution: signaling, dimerization, and mechanism. Biochemistry. 46: 3614–3623. [PubMed: 17319691]

Kloek AP, Yang J, Mathews FS, Frieden C, Goldberg DE. 1994; The tyrosine B10 hydroxyl is crucial for oxygen avidity of Ascaris hemoglobin. J Biol Chem. 269: 2377–2379. [PubMed: 8300562]

Kundu S, Hargrove MS. 2003; Distal heme pocket regulation of ligand binding and stability in soybean leghemoglobin. Proteins. 50: 239–248. [PubMed: 12486718]

Kurokawa H, Lee DS, Watanabe M, Sagami I, Mikami B, Raman CS, Shimizu T. 2004; A redox-controlled molecular switch revealed by the crystal structure of a bacterial heme PAS sensor. J Biol Chem. 279: 20186–20193. [PubMed: 14982921]

Liu YC, Machuca MA, Beckham SA, Gunzburg MJ, Roujeinikova A. 2015; Structural basis for amino-acid recognition and transmembrane signalling by tandem Per-Arnt-Sim (tandem PAS) chemoreceptor sensory domains. Acta Crystallogr D Biol Crystallogr. 71: 2127–2136. [PubMed: 26457436]

Machuca MA, Johnson KS, Liu YC, Steer DL, Ottemann KM, Roujeinikova A. 2017; *Helicobacter pylori* chemoreceptor TlpC mediates chemotaxis to lactate. Sci Rep. 7: 14089. [PubMed: 29075010]

Moglich A, Ayers RA, Moffat K. 2009; Structure and signaling mechanism of Per-ARNT-Sim domains. Structure. 17: 1282–1294. [PubMed: 19836329]

Nishiyama S, Suzuki D, Itoh Y, Suzuki K, Tajima H, Hyakutake A, Homma M, Butler-Wu SM, Camilli A, Kawagishi I. 2012; Mlp24 (McpX) of *Vibrio cholerae* implicated in pathogenicity functions as a chemoreceptor for multiple amino acids. Infect Immun. 80: 3170–3178. [PubMed: 22753378]

Nishiyama S, Takahashi Y, Yamamoto K, Suzuki D, Itoh Y, Sumita K, Uchida Y, Homma M, Imada K, Kawagishi I. 2016; Identification of a *Vibrio cholerae* chemoreceptor that senses taurine and amino acids as attractants. Sci Rep. 6: 20866. [PubMed: 26878914]

Otwinowski Z, Minor W. 1997; Processing of X-ray diffraction data collected in oscillation mode. Macromolecular Crystallography, Pt A. 276: 307–326.

Park SY, Borbat PP, Gonzalez-Bonet G, Bhatnagar J, Pollard AM, Freed JH, Bilwes AM, Crane BR. 2006; Reconstruction of the chemotaxis receptor-kinase assembly. Nat Struct Mol Biol. 13: 400–407. [PubMed: 16622408]

Parkinson JS. 1978; Complementation analysis and deletion mapping of *Escherichia coli* mutants defective in chemotaxis. J Bacteriol. 135: 45–53. [PubMed: 353036]

Rebbapragada A, Johnson MS, Harding GP, Zuccarelli AJ, Fletcher HM, Zhulin IB, Taylor BL. 1997; The Aer protein and the serine chemoreceptor Tsr independently sense intracellular energy levels and transduce oxygen, redox, and energy signals for *Escherichia coli* behavior. Proc Natl Acad Sci USA. 94: 10541–10546. [PubMed: 9380671]

Ringgaard S, Hubbard T, Mandlik A, Davis BM, Waldor MK. 2015; RpoS and quorum sensing control expression and polar localization of *Vibrio cholerae* chemotaxis cluster III proteins in vitro and in vivo. Mol Microbiol. 97: 660–675. [PubMed: 25989366]

Sawai H, Sugimoto H, Shiro Y, Ishikawa H, Mizutani Y, Aono S. 2012; Structural basis for oxygen sensing and signal transduction of the heme-based sensor protein Aer2 from *Pseudomonas aeruginosa*. Chem Commun (Camb). 48: 6523–6525. [PubMed: 22622145]

Schuster M, Hawkins AC, Harwood CS, Greenberg EP. 2004; The *Pseudomonas aeruginosa* RpoS regulon and its relationship to quorum sensing. Mol Microbiol. 51: 973–985. [PubMed: 14763974]

Selvaraj P, Gupta R, Peterson KM. 2015; The *Vibrio cholerae* ToxR regulon encodes host-specific chemotaxis proteins that function in intestinal colonization. SOJ Microbiol Infect Dis. 3: 1–5.

Sudhamsu J, Kabir M, Airola MV, Patel BA, Yeh SR, Rousseau DL, Crane BR. 2010; Co-expression of ferrochelatase allows for complete heme incorporation into recombinant proteins produced in *E. coli*. Protein Expr Purif. 73: 78–82. [PubMed: 20303407]

Taylor BL, Watts KJ, Johnson MS. 2007; Oxygen and redox sensing by two-component systems that regulate behavioral responses: behavioral assays and structural studies of Aer using in vivo disulfide cross-linking. Methods Enzymol. 422: 190–232. [PubMed: 17628141]

Watts KJ, Sommer K, Fry SL, Johnson MS, Taylor BL. 2006; Function of the N-terminal cap of the PAS domain in signaling by the aerotaxis receptor Aer. J Bacteriol. 188: 2154–2162. [PubMed: 16513745]

Watts KJ, Taylor BL, Johnson MS. 2011; PAS/poly-HAMP signalling in Aer-2, a soluble haem-based sensor. Mol Microbiol. 79: 686–699. [PubMed: 21255112]

Yang J, Kloek AP, Goldberg DE, Mathews FS. 1995; The structure of Ascaris hemoglobin domain I at 2.2 A resolution: molecular features of oxygen avidity. Proc Natl Acad Sci USA. 92: 4224–4228. [PubMed: 7753786]

Yu HS, Saw JH, Hou S, Larsen RW, Watts KJ, Johnson MS, Zimmer MA, Ordal GW, Taylor BL, Alam M. 2002; Aerotactic responses in bacteria to photoreleased oxygen. FEMS Microbiol Lett. 217: 237–242. [PubMed: 12480110]

Yukl ET, Ioanoviciu A, Nakano MM, de Montellano PR, Moenne-Loccoz P. 2008; A distal tyrosine residue is required for ligand discrimination in DevS from *Mycobacterium tuberculosis*. Biochemistry. 47: 12532–12539. [PubMed: 18975917]

Zhang Z, Hendrickson WA. 2010; Structural characterization of the predominant family of histidine kinase sensor domains. J Mol Biol. 400: 335–353. [PubMed: 20435045]

Zhou Q, Ames P, Parkinson JS. 2011; Biphasic control logic of HAMP domain signalling in the *Escherichia coli* serine chemoreceptor. Mol Microbiol. 80: 596–611. [PubMed: 21306449]

Zoltowski BD, Schwerdtfeger C, Widom J, Loros JJ, Bilwes AM, Dunlap JC, Crane BR. 2007; Conformational switching in the fungal light sensor Vivid. Science. 316: 1054–1057. [PubMed: 17510367]

ABBREVIATED SUMMARY

In this study we show that *V. cholerae* Aer2 is an O_2 receptor with two related but functionally divergent PAS-heme domains. PAS2 is an O_2 sensor that stabilizes O_2 binding via a conserved Trp residue, whereas PAS1 is a signal modulator that binds O_2 to regulate signaling from PAS2. O_2 binding to PAS1 required at least one of two heme pocket residues: the conserved Trp or a specific Tyr residue.

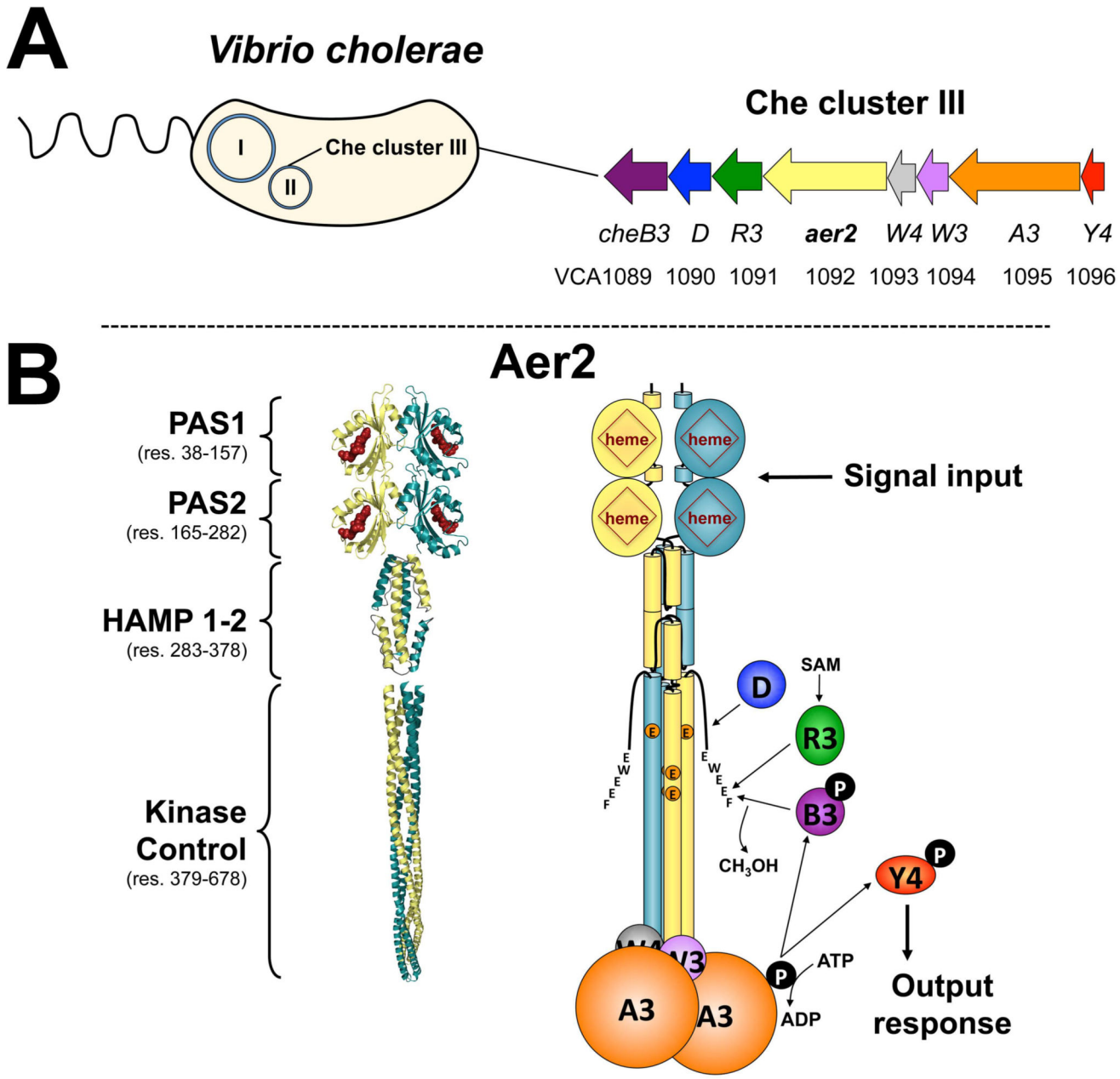

Fig. 1. *V. cholerae* chemosensory cluster III and the proposed structure of *Vc*Aer2

A. *V. cholerae* chemosensory (Che) cluster III resides on chromosome II and encodes a complete chemosensory system. This includes a chemoreceptor (Aer2), a histidine kinase (CheA3), two coupling proteins (CheW3 and W4), a response regulator (CheY4), and three adaptation enzymes (CheR3, D and B3).

B. The proposed structure of a *Vc*Aer2 dimer (left) and the cluster III chemosensory pathway (right). *Vc*Aer2 is predicted to contain two N-terminal PAS domains (PAS1 and PAS2), a di-HAMP unit (HAMP 1–2), and a kinase control module that is typical of methyl-accepting chemoreceptors [containing three putative methylation sites: EEE, residues 414, 421 and 603, and a C-terminal pentapeptide sequence (EWEEF) for the binding of adaption

enzymes]. In the left panel, PAS1 and PAS2 are modeled on the structure of *P. aeruginosa* Aer2 PAS [PDB code: 4HI4, (Airola *et al.*, 2013a)], the di-HAMP unit is modeled on the structure of *P. aeruginosa* Aer2 HAMP 2–3 [PDB code: 3LNR, (Airola *et al.*, 2010)], and the kinase control module is modeled on the structure of MCP_{1143C} [PDB code: 2CH7, (Park *et al.*, 2006)]. *Vc*Aer2 signaling is proposed to activate CheA3 autophosphorylation, which in turn phosphorylates CheY4, which purportedly regulates the response from the cluster III chemosensory system. *Vc*Aer2 signaling is modulated by the adaptation enzymes CheR3, D and B3, which bind the C-terminal pentapeptide EWEEF and/or the kinase control module to modify the methylation status of *Vc*Aer2. Abbreviation: SAM, *S*-adenosylmethionine.

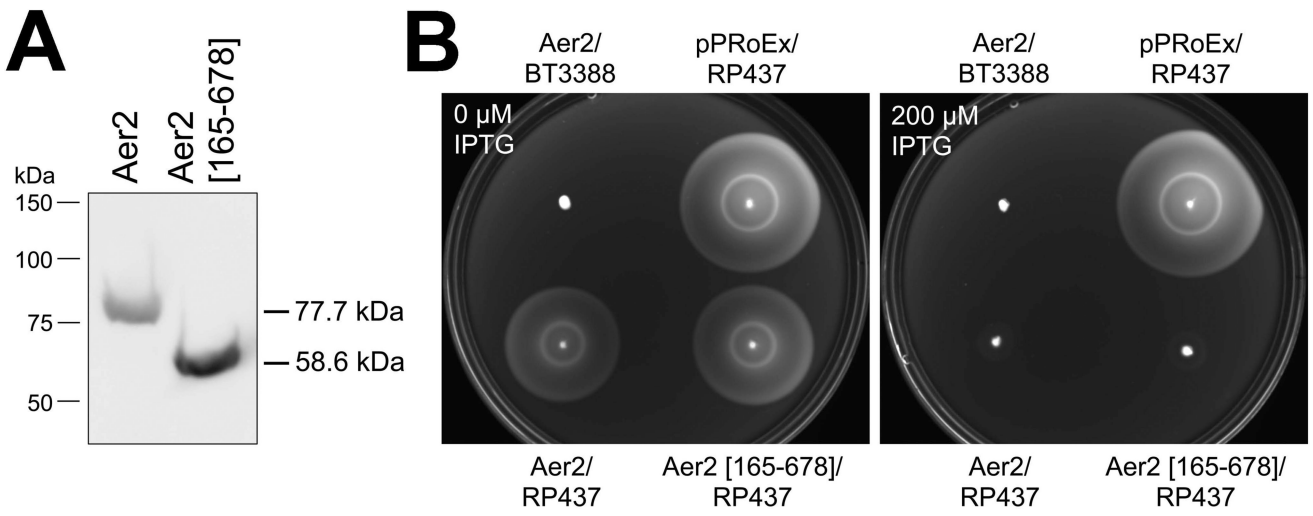

Fig. 2. Expression of *Vc*Aer2 in *E. coli* and its effect on *E. coli* chemotaxis

A. Full-length *Vc*Aer2 and *Vc*Aer2 [165–678] expression in *E. coli* BT3388 after induction with 50 μM IPTG. Full-length *Vc*Aer2 is stably expressed in *E. coli*, although *Vc*Aer2 [165–678] (ΔPAS1) has a higher steady-state level (see Fig. S2A).

B. *E. coli* BT3388 and *E. coli* RP437 expressing full-length *Vc*Aer2 or *Vc*Aer2 [165–678] in tryptone soft agar with 0 or 200 μM IPTG. BT3388 lacks the five native chemoreceptors of *E. coli*, whereas RP437 is a WT *E. coli* chemotaxis strain. Plates were incubated at 30 °C for 9 h. *Vc*Aer2 does not induce chemotaxis ring formation in *E. coli* BT3388, but disrupts chemotaxis ring formation by WT *E. coli* chemoreceptors (the outer Tsr serine ring and the inner Tar aspartate ring). Adding 25 μg ml^{-1} ALA to the plates (to assist heme incorporation in *Vc*Aer2) made no difference to the appearance of the colonies compared to colonies in plates without ALA (not shown).

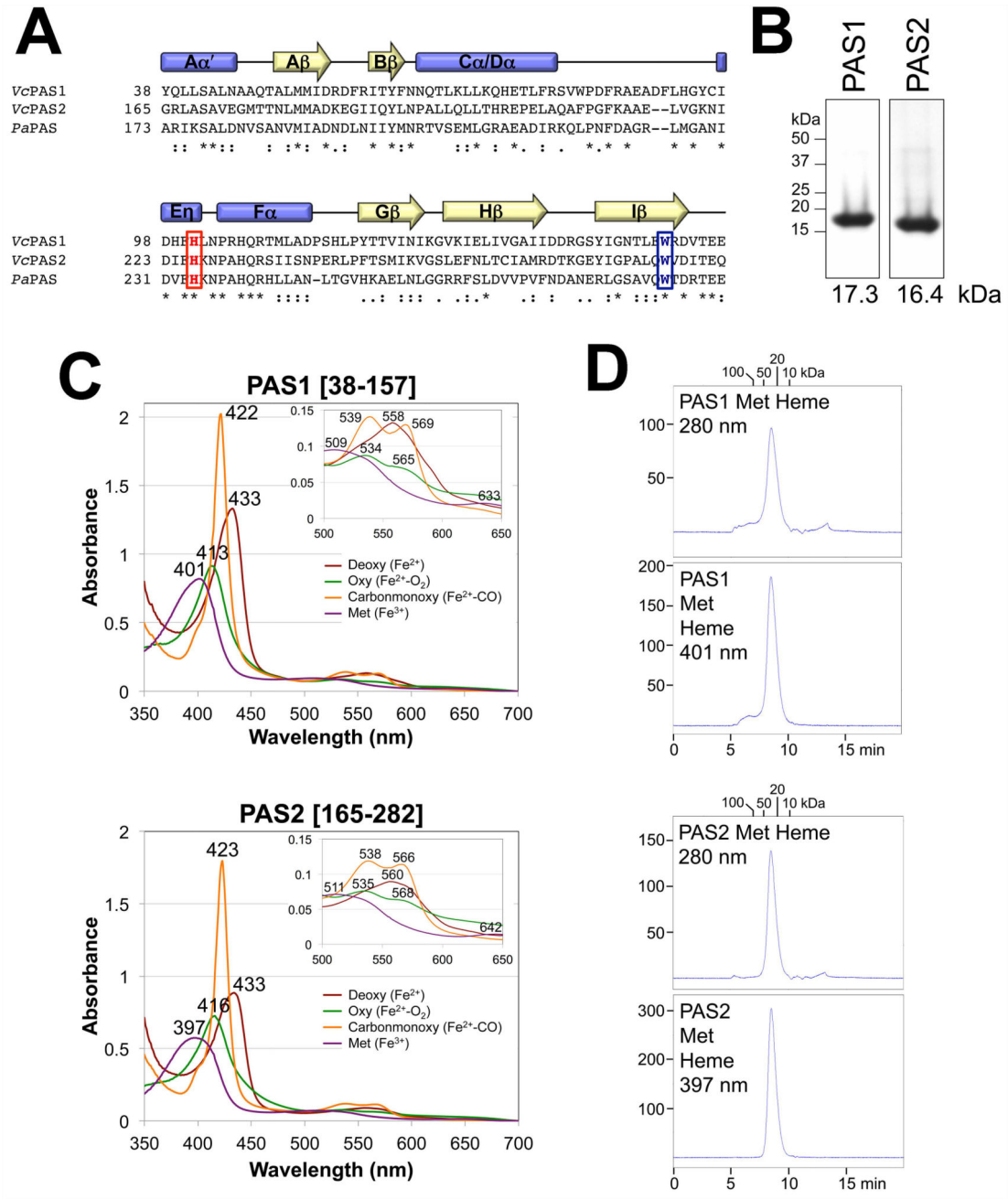

Fig. 3. Secondary structure, heme binding and oligomeric state of the PAS1 and PAS2 domains of *Vc*Aer2

A. Sequence alignment of PAS1 and PAS2 from *V. cholerae* Aer2 and *Pa*PAS from *P. aeruginosa* Aer2 as generated in ClustalW. The conserved His that coordinates heme in *Pa*PAS, and the conserved Trp that stabilizes O_2-binding to *Pa*PAS, are highlighted red and blue, respectively. Secondary structure elements are based on the solved structures of *Pa*PAS (Sawai *et al.*, 2012, Airola *et al.*, 2013a). Stars indicate conserved residues, colons indicate similar amino acids, and periods indicate amino acids with weakly similar properties.

B. Coomassie-stained SDS-PAGE of 5 μg of purified PAS1 [38–157] and PAS2 [165–282] peptides.

C. Absorption spectra of 10 μM purified PAS1 and PAS2 domains in the reduced (deoxy), oxidized (met), carbon monoxide-bound (carbonmonoxy) and oxygen-bound (oxy) states. The wavelength for each absorbance maximum is indicated. The insert shows an expanded view of peaks between 500 and 650 nm.

D. Elution profiles of isolated PAS1 and PAS2 peptides (200 μg) in their met-heme states during size-exclusion chromatography. Elution profiles are shown in arbitrary units at 280 nm to reveal total protein content (top panels) and at 401 nm (PAS1) or 397 nm (PAS2) to detect the elution of met-heme (bottom panels). The area under the peak for PAS2 is 97% the area of PAS1. Fractions were removed and analyzed by Western blotting; in all cases, PAS peptide co-eluted with the heme (not shown).

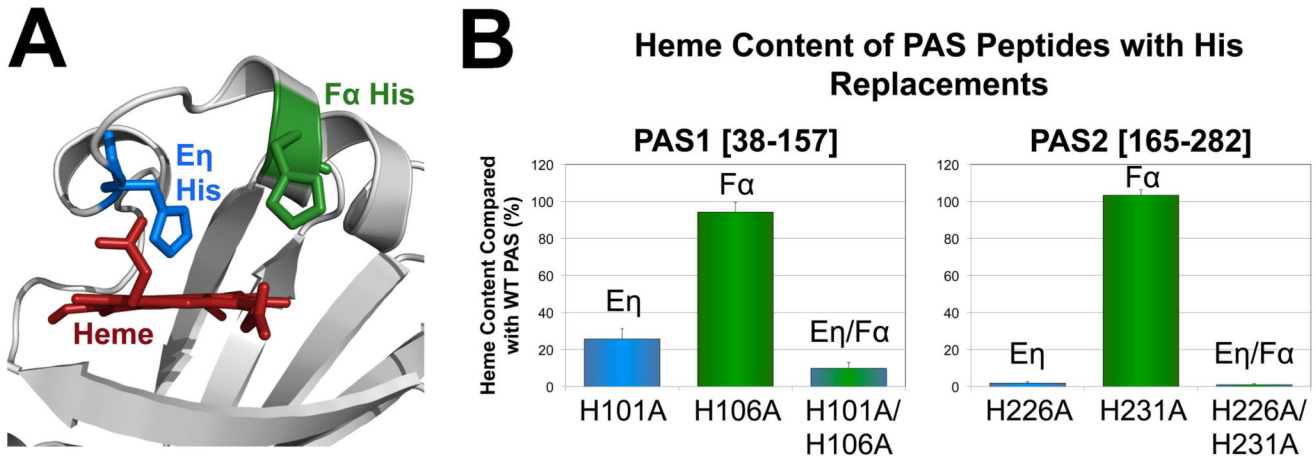

Fig. 4. Heme coordination in the PAS1 and PAS2 domains of *Vc*Aer2

A. Location of the Eη and Fα His side chains on the PAS2-W276L structure (see Fig. 7). The distance from the Fe atom to the Eη His NE2 atom is 2.5 Å, whereas the distance from the Fe atom to the Fα His NE2 atom is 10.5 Å.

B. Average heme content of PAS1 [38–157] and PAS2 [165–282] peptides with Eη and Fα His replacements, given as a percentage of WT PAS heme content, corrected for peptide concentration. Error bars represent standard deviations from two to three experiments. The heme content of PAS1-H101A is significantly different from the heme content of PAS1-H101A/H106A ($P < 0.05$).

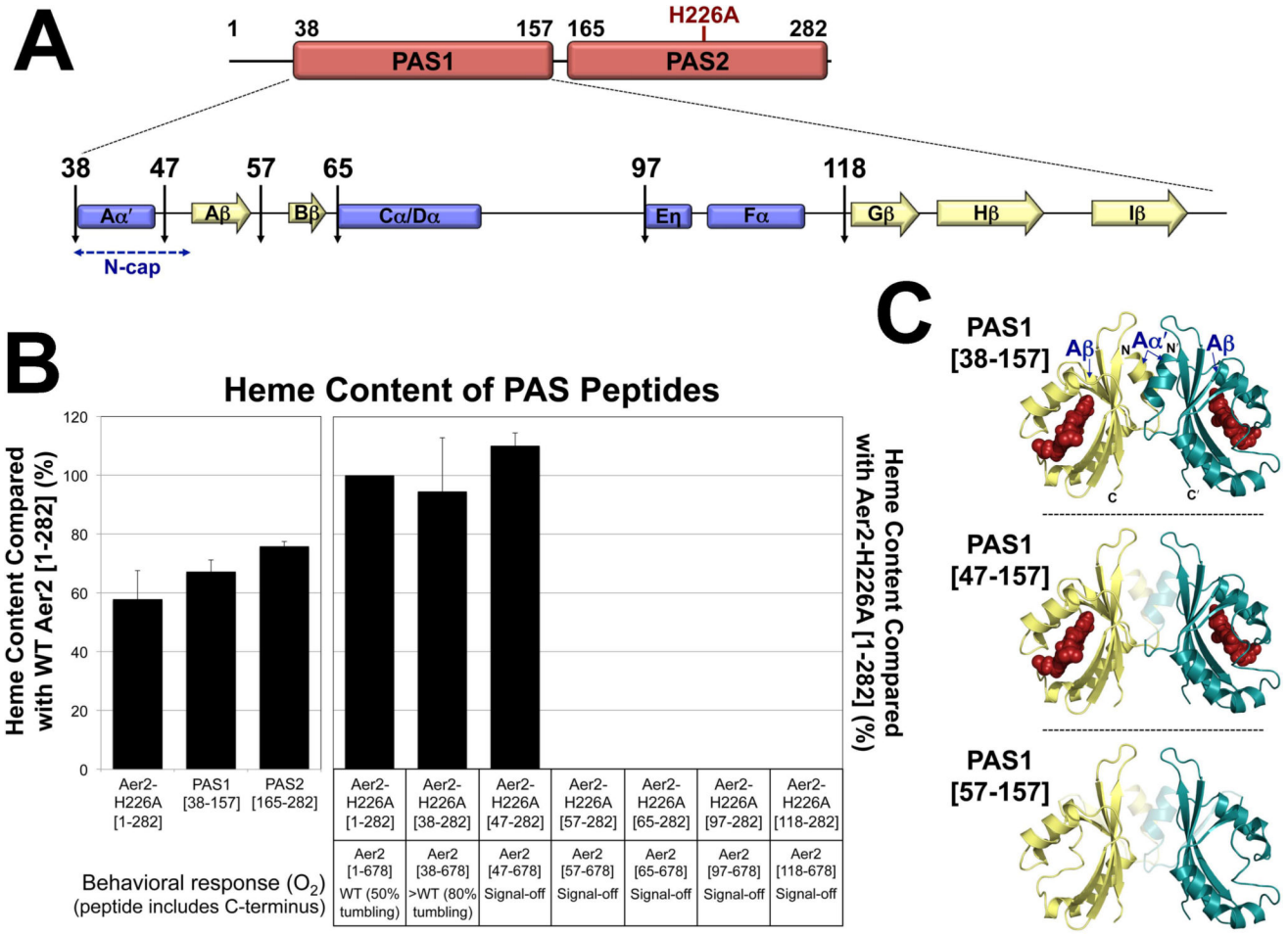

Fig. 5. Effects of N-terminal truncations on PAS1 heme binding and *Vc*Aer2 behavior

A. Cartoon of PAS1-PAS2 (res. 1–282), the predicted secondary structure elements of PAS1, and locations of the N-terminal truncations.

B. Average heme content of PAS peptides, given as a percentage of the heme content in either WT *Vc*Aer2 [1–282] (left panel) or *Vc*Aer2-H226A [1–282] (right panel), corrected for peptide concentration. Error bars represent standard deviations from two to four experiments. The amount of heme bound to *Vc*Aer2-H226A [1–282] (i.e., heme bound to PAS1 in the presence of heme-less PAS2, left panel) is not significantly different from the amount of heme bound to PAS1 [38–157] ($P = 0.3$). The behavioral responses of BT3388 cells expressing *Vc*Aer2 mutants with N-terminal truncations are provided beneath the bar graph. The >WT mutant (*Vc*Aer2 [38–678]) exhibited ~80% tumbling in air compared with ~50% for WT *Vc*Aer2, whereas the signal-off mutants exhibited smooth-swimming behavior (2–5% tumbling) in both air and N_2.

C. PAS1 dimer model based on the structure of *P. aeruginosa* Aer2 PAS (Airola *et al.*, 2013a) showing the truncations that retained heme (top and center panels) and the shortest truncation that no longer retained heme (57–157, bottom panel). In each case, the translucent region represents the N-terminal residues (Aα′ helix, Aα-Aβ loop, and Aβ strand) that were sequentially deleted from PAS1.

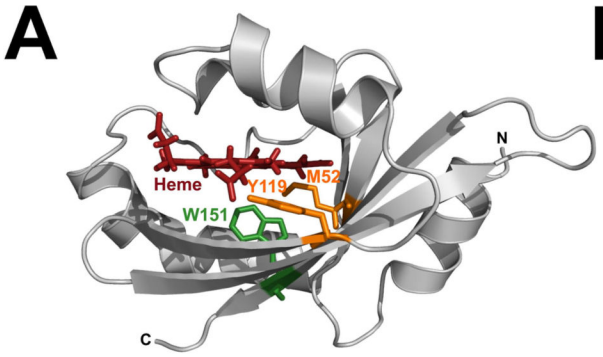

B

Aer2 O_2 Behavioral Responses

Behavioral Response (O_2)	Amino Acid Substitution
WT behavior	H106A, W151P, V, H231A
Signal-off	W151E, R, Y119L/W151L, W276V
Signal-off biased	Y119L, W151C, L, N, H226A, W276C
Signal-on biased	W151F, W276F, L
>WT behavior	M52L, H101A, W151G, S, T

D

Dissociation Constants

PAS1 [38-157]	O_2 K_d (μM)	CO K_d (μM)
WT PAS1	12	7
Y119L	13	8
W151C	14	5
W151F	14	4
W151G	9	6
W151L	17	5
W151P	9	4
W151S	7	4
W151T	8	7
W151V	12	7
Y119L/W151L	-	8

PAS2 [165-282]	O_2 K_d (μM)	CO K_d (μM)
WT PAS2	19	5
W276C	-	4
W276F	17	7
W276L	-	5
W276V	-	8
Aer2 [165-678]	20	2

C

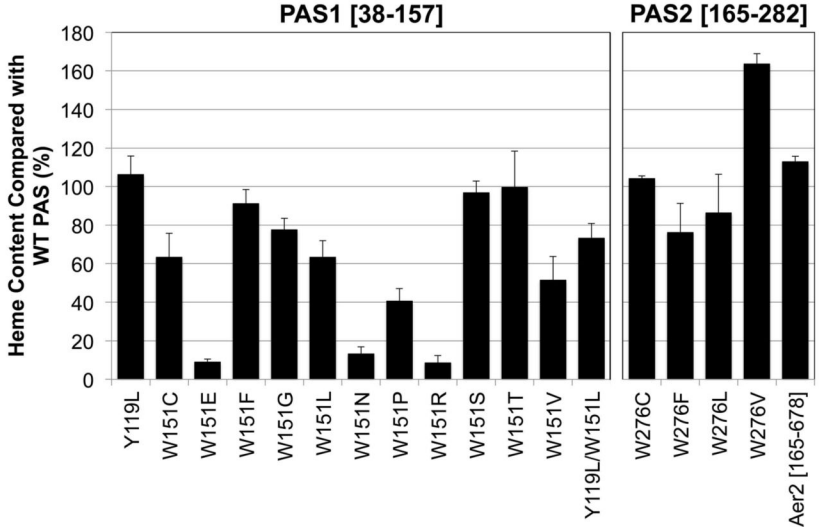

Fig. 6. *Vc*Aer2 PAS mutant behavior, heme content and gas-binding affinities

A. The location of PAS1 residues M52, Y119 and W151 based on the structure of the *P. aeruginosa* Aer2 PAS domain (Airola *et al.*, 2013a).

B. The behavior of full-length *Vc*Aer2 mutants in BT3388 compared with WT *Vc*Aer2 (which caused ~50% tumbling in air and ~2% tumbling in N_2). Mutants with WT behavior exhibited 30–55% tumbling in air; signal-off mutants exhibited 2–5% tumbling in air; signal-off biased mutants exhibited 10–25% tumbling in air; >WT mutants exhibited 80–98% tumbling in air. All of these mutants exhibited ~2% tumbling in N_2. In contrast, the signal-on-biased mutants caused 95–98% of cells to tumble in air, but had 20–50 sec delayed

smooth-swimming (~2% tumbling, W151F and W276L) or incomplete smooth swimming (50–80% tumbling, W276F) responses in N_2.

C. Average heme content of PAS peptides with amino acid substitutions, given as a percentage of WT PAS1 (left panel) or WT PAS2 (right panel) heme content, corrected for peptide concentration. *Vc*Aer2 [165–678] heme content is given as a percentage of full-length *Vc*Aer2 [1–678] heme content. Values below 15% indicate a substantial heme-binding defect. Error bars represent standard deviations from two to five experiments.

D. PAS peptide O_2 and CO binding affinities. A dash indicates that O_2-bound spectra were not observed, so no binding affinity was determined.

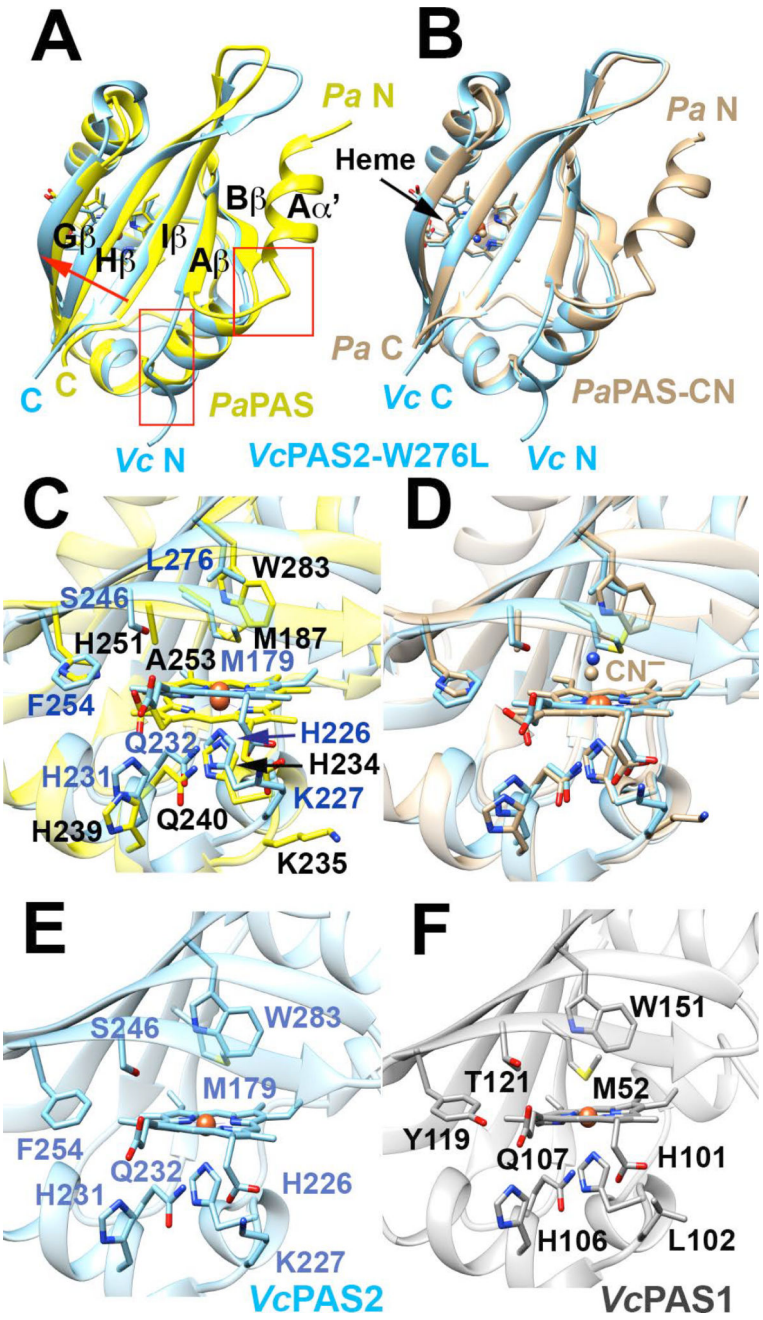

Fig. 7. The structure of PAS2-W276L and its relationship to *Pa*PAS structures and WT PAS1 and PAS2 homology models

A–B. Superposition of PAS2-W276L (A; PDB code: 6CEQ, blue) and *Pa*PAS in the unliganded ferric-heme form (A; PDB code: 4HI4, yellow) and the CN^--bound form (B; PDB code: 3VOL, brown). The structures of PAS2-W276L and both *Pa*PAS structures are similar, except that the Aα′ helix is dissociated and unstructured in PAS2-W276L (red boxes). However, PAS2-W276L is most similar to the ligand bound form of *Pa*PAS, with the β-sheet shifted slightly relative to the ferric form of *Pa*PAS (A; red arrow).

C–D. Superposition of the heme-binding pockets of PAS2-W276L (blue) and *Pa*PAS in the unliganded ferric-heme form (C; yellow) and CN^--bound form (D; brown).

E–F. Comparison of the heme pockets of WT PAS2 (E) and WT PAS1 (F) homology models. Modeling of the WT PAS2 structure and PAS1 domain was accomplished in SWISS-MODEL using the PAS2-W276L structure as a template in both cases.